Melt hybridization and metasomatism triggered by syn-magmatic faults within the Oman ophiolite: A clue to understand the genesis of the dunitic mantle-crust transition zone

Mathieu Rospabé, Mathieu Benoit, Georges Ceuleneer, Mary-Alix Kaczmarek, Florent Hodel

Melt hybridization and metasomatism triggered by syn-magmatic faults within the Oman ophiolite: a clue to understand the genesis of the dunitic mantle-crust transition zone

Mathieu Rospabé [a,*], Mathieu Benoit [a], Georges Ceuleneer [a], Mary-Alix Kaczmarek [a], Florent Hodel [a]

[a] Géosciences Environnement Toulouse (GET), Observatoire Midi Pyrénées, Université de Toulouse, CNRS, IRD, 14 avenue E. Belin, F-31400 Toulouse, France

* Corresponding author. E-mail address: mathieu.rospabe@get.omp.eu

Abstract

On Earth, most of the critical processes happen at the frontiers between envelopes and especially at the Moho between the mantle and the crust. Beneath oceanic spreading centres, the dunitic transition zone (DTZ) appears as a major interface between the upwelling and partially molten peridotitic mantle and the accreting gabbroic lower crust. Better constraints on the processes taking part in the DTZ allows improved understanding of the interactions between silicate melts and hydrated fluids, which act competitively to generate the petrological Moho. Here we combine mineral and whole rock major and trace element data with a structural approach along three cross-sections up to 300 m thick above the fossil Maqsad mantle diapir (Oman ophiolite) in order to understand the vertical organization of the DTZ with depth. Our results highlight that most of the faults or fractures cross-cutting the DTZ were ridge-related and active at an early, high temperature magmatic stage. Chemical variations along the cross-sections define trends with a characteristic vertical scale of few tens

of meters. There is a clear correlation between the chemical variation pattern and the distribution of fault zones, not only for fluid-mobile elements but also for immobile elements such as REE and HFSE. Faults, despite displaying very limited displacements, enhanced both melt migration and extraction up to the crust and deep hydrothermal fluids introduction down to the Moho level. We propose that these faults are a vector for upwelling melt modification by hybridization, with hydrothermal fluids and/or silicic hydrous melts, and crystallization. Infiltration of these melts or fluids in the country rock governs part of the gradational evolutions recorded in composition of both the olivine matrix and interstitial phases away from faults. Finally, these faults likely control the thermal structure of the mantle-crust transition as evidenced by the spatial distribution of the crystallization products from percolating melts, organizing the transition zone into pure dunites to impregnated dunites horizons. In this context, the DTZ appears as a reactive interface that developed by the combination of three primary processes: tectonics, magmatism and deep, high temperature hydrothermal circulations. Accordingly, these features fundamentally contribute to the variable petrological and geochemical organization of the DTZ and possibly of the lower crust below oceanic spreading centers, and may be a clue to interpret part the heterogeneity observed in MORB signatures worldwide.

Keywords

Oman ophiolite, dunitic mantle-crust transition zone, syn-magmatic faulting, melt-rock reactions, high temperature hydrothermalism, melt hybridization

1. Introduction

The oceanic crust is generated at spreading centers where extensive thermal and chemical exchanges occur between the mantle, the crust and the external envelopes. Crustal accretion at

oceanic spreading centres is not a steady state process, proceeding by the cyclic succession of magmatic and magma-starved episodes, whatever the spreading rate (e.g. Gente et al., 1995; Sinton et al., 2002; Yeo et al., 2016). During periods of magmatic quiescence, the front of hydrothermal systems can deepen significantly, a propagation likely triggered by normal faulting and detachment faults. This leads to the efficient cooling and alteration of the mafic-ultramafic substratum and to elements mobilization and redistribution (e.g. German et al., 2016 among recent studies), and therefore impacts chemical exchanges happening along oceanic spreading centers. In addition, there is accumulating evidence for magmatism-hydrothermalism relationships beneath oceanic spreading centres, in temperature conditions high enough to induce the re-melting of previously hydrated rocks (e.g. Amri et al, 1996; Benoit et al, 1999; Koepke et al., 2005; Zhang et al., 2017 and references therein) or allowing crystallizing magmas and hydrothermal fluids to interact (e.g. Abily et al., 2011; Rospabé et al., 2017). The Oman ophiolite has been shown to be an excellent analogue of present-day spreading centres to study deep-seated hydrothermal processes, whatever its precise tectonic setting (i.e. Mid-Ocean Ridge vs. arc-related basin) (e.g. Bosch et al., 2004; Currin et al., 2018; France et al., 2009, 2013; Gilgen et al., 2016; Python et al., 2007; Zihlmann et al., 2018).

In the Oman ophiolite, petrological and isotopic studies have shown that the crust was affected by hydrothermal circulations ranging from greenschist to upper amphibolite/granulite facies (e.g. Bosch et al., 2004; Gregory and Taylor, 1981; Koepke et al., 2005; Nehlig and Juteau, 1988; Currin et al., 2018). The formation of diopsidite and rodingite dikes likewise involves high temperature hydrothermal fluids circulating down to the Moho and even below (Akizawa et al., 2011; Python et al., 2007). Most of these alteration features post-date the crystallization stage and are introduced at depth via fracture networks (Nehlig and Juteau,

1988; Reuber, 1988). However, when normal faults develop early and root at Moho level, seawater can locally reach the incompletely crystallized lower crust (Abily et al., 2011).

The dunitic transition zone (DTZ) from the Maqsad area (Oman ophiolite), like dunites from other ophiolites (e.g. Quick, 1981; Ceuleneer and Le Sueur, 2008; Sanfilippo et al., 2014; 2017), displays extensive petrological and geochemical variations that result from the overprint of several magmatic processes: incongruent melting of harzburgite orthopyroxenes (i.e. "dunitization"), chemical re-equilibration between the olivine matrix and percolating melts, refertilization by variably evolved melt batches (Rospabé et al, 2018a). In addition to interstitial plagioclase and clinopyroxene reflecting the fractionation from a percolating MORB (Abily and Ceuleneer, 2013; Koga et al., 2001), the occurrence of orthopyroxene, amphibole, diopside and garnet, both in interstitial position and - with mica - included in chromite, highlights the early contribution of a more exotic, hydrated and silica-richer component that variably mixed with the MORB (Rospabé et al., 2017). The composition and bottom to top distribution of minerals that crystallized in response to this hybridization process calls for a hydrothermal origin of the water rather than a deep, subduction-related origin. Chromitites associated to minerals of high temperature hydrothermal origin are ubiquitous at Moho level in the Oman ophiolite. Accordingly, if can be inferred that this process affected the whole ophiolite. However, the way in which this hydrated component was introduced at high temperature within the DTZ remains poorly constrained. In order (1) to specify the petrological, geochemical and tectonic structuration of the DTZ beneath oceanic spreading centres and (2) to decipher the enigmatic relationships between the tectonic history of the DTZ and its imbricated magmatic and hydrothermal signatures, we investigated a portion of the paleo-ridge axis related to the Maqsad mantle diapir. This area appears densely faulted according to previous geological maps (Amri, 1995; Rabu et al., 1986). Our

results highlight that faults were active early at Moho level, since the magmatic stage, and that they conditioned the petrological and geochemical organization of the DTZ, and probably of the overlying lower crust, by exerting a strong control on the mantle harzburgite dunitization and on melts migration and crystallization.

2. Geological setting

2.1. Geology of the Oman ophiolite

The Oman ophiolite is the largest (~500 × 50 km) remaining oceanic lithosphere fragment from the Tethyan ocean. It formed along a (possibly fast) spreading ridge ~95-97 million years ago (e.g. Boudier et al., 1988; Rioux et al., 2013 and references therein). The synoptic mapping of plastic deformation structures preserved in mantle peridotites allowed characterizing vertical flow patterns in several areas; they were interpreted as upwelling asthenospheric diapirs beneath the former oceanic ridge axis along which the lithosphere accreted (Ceuleneer et al., 1988; Jousselin et al., 1998; Nicolas et al., 1988). The paleo-ridge axis orientation evolves from a N-S direction in the north of the ophiolite to NW-SE in the south, although exceptions to this general tendency can be observed locally (e.g. MacLeod and Rothery, 1992; Nicolas et al., 1988; Pallister, 1981). The mapping of the nature of the dikes cropping out within the mantle section (Python and Ceuleneer, 2003) has evidenced a MORB-like environment mainly in the SE massifs of the ophiolite, together with other restricted occurrences, while a depleted calc-alkaline magmatism is observed elsewhere.

2.2. The Sumail Massif

The Sumail massif, located in the SE of the ophiolite and focus of the present study, exposes the well preserved Maqsad fossil mantle diapir and its associated N130 trending paleo-spreading centre (Ceuleneer, 1991; Ceuleneer et al., 1988; Jousselin et al., 1998) (Fig. 1A). It

126 fed the largest (~80 × ~30 km) MORB area of the Oman ophiolite (Python and Ceuleneer,
127 2003). The intense igneous activity related to the diapir is witnessed by abundant melt
128 migration structures cropping out in mantle harzburgites (Benoit et al., 1996; Ceuleneer et al.,
129 1996; Python and Ceuleneer, 2003), by the 300-400 m thick DTZ in between mantle and
130 crustal sequences (Abily and Ceuleneer, 2013; Boudier and Nicolas, 1995; Ceuleneer and
131 Nicolas, 1985; Jousselin et al., 1998; Rospabé, 2018), and by abundant chromitite ore bodies
132 (Ceuleneer and Nicolas, 1985). The Sumail massif was slightly tilted by post-accretion
133 tectonism, its regional dip does not exceed 10° to the SE.
134
135 Two sets of highly dipping faults confer to the Maqsad area its more salient tectonic and
136 morphologic features according to geological maps (Amri, 1995; Rabu et al., 1986): (1) One
137 strikes N130 and is parallel to the strike of the sheeted dike complex in this area, i.e. parallel
138 to the regional orientation of the inferred paleo-ridge axis (Ceuleneer, 1991; MacLeod and
139 Rothery, 1992; Pallister, 1981) (Fig. 1A). This system may reasonably be related to the
140 former spreading activity since it has been evidenced that N130-trending faults have generally
141 a normal offset and have locally disturbed crystallization sequences in the lowermost gabbroic
142 crust in this area, in association with hydrothermal fluids (Abily et al., 2011). N130 is also the
143 azimuth of the olivine gabbro dykes in the mantle section of the Maqsad area (Ceuleneer et al,
144 1996). (2) The other fault system strikes N160 to N-S, parallel to the Muqbariah high
145 temperature mylonitic shear zone (Amri et al., 1996; Ceuleneer, 1991) (Fig. 1A). Moving
146 away from the diapir, the diverging mantle flow is limited to the SW by the Muqbariah shear
147 zone, itself injected by numerous dikes from a depleted andesite kindred, contrasting with the
148 MORB signature of the dykes present in the diapir and at its immediate periphery, and to the
149 NE by an area injected by pegmatitic dikes and intrusions from the same andesitic melts
150 (Amri, 1995; Amri et al., 1996; Benoit et al., 1999). It has been proposed on the basis of

151 geological and isotopic arguments that these intrusions and dykes originated from
152 “lithospheric” melts generated by the remelting of hydrothermally altered peridotites at an
153 early stage of interaction between the lithosphere and the rising Maqsad diapir (Amri et al.,
154 1996; Benoit et al., 1999; Clénet et al., 2010). Although no detailed study was conducted yet
155 about the interplay between SW-NE spreading and shearing along N160-180 shear zones, first
156 evidence show they took place early during the Maqsad ridge development.
157

158 **3. Organization of the DTZ along the Maqsad paleo-ridge axis**

159 We report here below on the structural, petrological and geochemical characteristics of three
160 cross-sections sampled through the Maqsad DTZ. These sections were selected among twenty
161 we explored in this area (Rospabé, 2018) because they particularly well illustrate the
162 interactions between early faulting and geochemical evolution of the DTZ. They were
163 collected along the inferred paleo-ridge axis northwest to the centre of the fossil diapir (Fig.
164 1A), with from north to south the sections #1, #2 and #3 (Fig. 1B, Supplementary Table S1).
165 The sampling was performed in a W-E orientation from the wadi Mahram to the west
166 (altitude ~635 m) to the top of the DTZ to the east, exposed at an altitude of ~1070 m in this
167 area (Fig. 1B). The sampling interval ranges from 10 to 20 m vertically. We adopted this
168 strategy in order to cross the two N130 and N165-180 trending fault systems cross-cutting the
169 DTZ. Chemical evolutions along the DTZ are presented for mineral and whole rock major
170 elements as well as for whole rock trace elements for a total of 125 samples. Mineral and
171 whole rock compositions are given in Supplementary Table S2 and Supplementary Table S3
172 respectively. Analytical methods are detailed in the Electronic Supplement 1.
173

174 *3.1. Tectonic structuration of the DTZ*

175 *3.1.1. The N130 fault system*

176 The N130 faults are regularly spaced by horizontal distances of ~250 meters on average. They
177 can be followed along strike on up to 2 km and have generally a dip of 65-70° toward the NE.
178 The cross-section #2 exposes conversely two successive faults with a dip toward the SW (Fig.
179 1B). The amplitude of the displacement along N130 faults has been established in a few cases
180 where they offset plurimetric troctolites intrusions: the movement is normal and the
181 displacement is limited to a few meters at most. A troctolite lens located about 1.5 km
182 westward of the considered cross-sections developed a strong high temperature deformation
183 along a N130.70NE normal fault (Fig. 2A), similarly to what was described at the base of the
184 crustal section near Maqsad (Abily et al., 2011). The N130 fault zones display clear brittle
185 features near the top of the DTZ and appear to be progressively rooted through the DTZ
186 where they evolve to serpentine and carbonate breccias. Brecciated zones reach up to about
187 10 meters in thickness concerning major faults. The alteration halo having affected the dunitic
188 wall rock does not exceed a few meters.
189
190 *3.1.2. The N165-180 fault system*
191 The N165-180 system accommodated a transtensional movement with a clear normal and
192 more subtle dextral components. This system is represented by two main discontinuities in the
193 explored area, the western N165-180-trending one making the contact between the mantle
194 section and the DTZ, and the easternmost ~N165 being internal to the DTZ (Fig. 1B):
195 - The westernmost N165-180 major discontinuity is organized as an asymmetric
196 graben-type structure limited by two N165.85E to vertical and N180.80W faults (Fig. 1B). It
197 induced the collapse of a layered troctolite unit down to the base of the DTZ, supporting a
198 significant normal movement. This system clearly evolved during a long time scale, starting
199 with early, syn- to sub-magmatic deformations - gabbros boudins, elongated mafic intrusions
200 (Fig. 2B) -, and becoming progressively affected by increasingly brittle fracturing as well as

by greenschist facies alteration of surrounding rocks. The schistosity within the N165.85E fault centre, making the contact between mantle harzburgites and DTZ dunites (Fig. 1B), points to an intense dextral movement similar to the dominant motion recorded by the Muqbariah mylonitic shear zone (Amri et al., 1996).

- The second system affecting the DTZ internally evolves from a N155.65NE direction to the south, along the cross-section #3, to a N170 sub-vertical orientation to the north along the two cross-sections #1 and #2 (Fig 1B). It accommodated a transtensional movement with a normal displacement much lower than along the westernmost system in regard to the absence of deformation in its centre. The strike-slip along this discontinuity is estimated to about 80 m at most regarding two N130 fault segments offset, with a dextral movement, north to the cross-section #1. Likewise, the geological map from Rabu et al. (1986) generally shows N130 faults cross-cut and shifted by the later N165 system. However, we also observed the reverse relationships in some locations with the disruption of N165-180 factures by later N130 faults, pointing out the contemporaneity of both systems.

Other minor N165-180 faults or fractures affecting the DTZ, few meters in width at most, become more abundant upsection. They confer a shale-like parting to the dunites while examination of thin section reveals no evidence of high-temperature mylonitic deformation (Fig. 2C). Shear sense indicators are poorly developed and vertical offsets seem to be restricted to a few meters, making of these fractures transtensional to purely extensional cracks. They are mostly subvertical or with a strong dipping generally to the west. Along these fractures, troctolite intrusions are affected by greenschist facies metamorphism while serpentine and carbonate developed into or parallel to the fracture plans in surrounding dunites. Along a companion N165.80W fault right to the west of the easternmost major discontinuity, a swarm of undeformed gabbro dikes oriented according to both N125.70NE and N105.60NE orientations cuts across the N165-trending schistosity, stressing on the early

226 fault development before melt percolation and fluids circulation and subsequent alteration
227 (Fig. 2C).
228
229 *3.2. Petrological sequences within the DTZ*
230 Previous studies described a highly variable mineralogical content within the Maqsad DTZ,
231 with dunites evolving from "pure", containing only olivine together with a few percent of
232 scattered chromite grains and rare, small clinopyroxene, to strongly impregnated (up to 30%
233 of interstitial minerals) (e.g. Abily and Ceuleneer, 2013; Boudier and Nicolas, 1995; Koga et
234 al., 2001). Impregnated dunites contain one or more interstitial mineral phases among
235 clinopyroxene, plagioclase, orthopyroxene, amphibole and other accessory minerals (e.g.
236 hydrothermal diopside, grossular garnet) (Rospabé et al., 2017). Hence, dunites from the
237 Maqsad DTZ are classified in the present study as pure dunites, cpx-bearing dunites, pl/cpx-
238 bearing dunites, opx/pl/cpx-bearing dunites and amph-bearing dunites (± opx/pl/cpx)
239 (Rospabé et al., 2018a).
240
241 The contacts between the main units composing the ophiolite are frequently faulted within the
242 studied area. Mantle harzburgites were not observed along the wadi Mahram except to the
243 west of the major westernmost N165 tectonic accident (Fig. 1B). The three sampled cross-
244 sections are entirely made of variably impregnated dunites and contain a high abundance of
245 troctolite intrusions upsection (Fig. 3). These intrusions, plurimetric in size and cumulative in
246 texture, display clear intrusive relationships at the contact with surrounding dunites showing
247 they were injected within the near-solidified DTZ. The cross-sections #1 and #3 present a
248 similar lithological succession, with a lower half part made of pure dunites and an upper part
249 widely impregnated. The transition from pure to impregnated portions corresponds to the
250 major easternmost ~N165 discontinuity. The pure dunitic lower units regularly contain small

size (100 μm at most) clinopyroxene or hybrid diopside (i.e. hybrid between igneous clinopyroxene and hydrothermal diopside; Rospabé et al., 2017) in interstitial position along olivine grain boundaries (Fig. 4A). We observed locally, approaching fault zones, a higher amount of chromite, occurring as schlierens and more rarely as massive dikes (Fig. 4B). Along the cross-section #1, clinopyroxene and a scarce amount of plagioclase progressively appear just above the major eastern N170 fault (Fig. 3). They become much more abundant together with the appearance of orthopyroxene and amphibole twenty meters above, in the uppermost section part, beyond a N130.60NE fault. Along the cross-section #3, clinopyroxene, plagioclase, orthopyroxene and amphibole appear all together above the N155 segment, directly in the southward continuity of the eastern ~N165 major discontinuity (Fig. 3). These mineral phases are observed all along the impregnated upper part. Plagioclase is slightly more abundant than clinopyroxene until a N175 fault zone, while clinopyroxene and orthopyroxene are more frequently observed above (Fig. 4C). Amphibole is unequally distributed along the section.

The cross-section #2, located midway from sections #1 and #3, does not respect this dichotomous structuration (Fig. 3). Interstitial amphibole, plagioclase and clinopyroxene are more frequent all along this section (Figs. 4D and E) while pure dunites are quite uncommon. Despite this erratic mineral distribution, amphibole appears more abundant in specific subsections, limited by both N130 and N165-N180 faults zones, while orthopyroxene is restricted to the uppermost level above a N130.55SW fault.

3.3. DTZ geochemical patterns

The olivine chemical content is highly variable in dunites collected along the Maqsad DTZ, with Fo and NiO contents varying from 93.2 to 85.7 and from 0.16 to 0.45 wt.% respectively.

276 The olivine composition does not correlate with the presence/abundance of other minerals
277 (Fig. 5A).
278 Pure dunites are characterized by U- or V-shaped REE patterns (La_{CN}/Sm_{CN} = 0.60-3.8;
279 Gd_{CN}/Yb_{CN} = 0.05-0.27) and by enrichment in LILE and positive Pb, Sr and Ti anomalies in
280 regard to REE in their extended trace element patterns (Fig. 6B). Impregnated samples
281 containing clinopyroxene, plagioclase, orthopyroxene and/or amphibole interstitially between
282 olivine grains generally show convex-upward REE patterns characterized by HREE to LREE
283 depletion (La_{CN}/Yb_{CN} = 0.02-0.42) (Fig. 6B).
284 Mineral and whole rock compositions as a function of the sampling altitude are shown in
285 figures 6 and 7 (see also the Electronic Supplement 2). The regional N130 and N165-180
286 faults are reported at the altitude they cut across each section respectively (see Figure 3 for
287 their dipping). Chemical variations are not randomly distributed from one sampling point to
288 another: they display progressive and successive increasing or decreasing evolutions
289 (depending on the regarded element) with inversions from a trend to another every hundred
290 meters approximately. In the following we propose to show how the different chemical trends
291 are related (1) to the samples modal composition, (2) to their position relative to fault zones,
292 or (3) if they are essentially cryptic (i.e. unrelated to lithological or structural features).
293
294 *3.3.1. Chemical trends related to lithological facies*
295 Mineral and whole rock chemical compositions are highly variable in the Maqsad DTZ
296 dunites (Rospabé et al., 2018a). Whole rock vertical composition evolutions are partly
297 controlled by the modal composition of the samples. High amount of interstitial phases
298 (essentially plagioclase and pyroxene), likely related to impregnation (Fig. 4), leads to an
299 increase in CaO and Li contents, in the Gd_{CN}/Yb_{CN} ratio and the concavity of REE patterns
300 ($\sqrt{(Sm_{CN} \times Gd_{CN})}/\sqrt{(Ce_{CN} \times Yb_{CN})}$ -1), and to a decrease in La_{CN}/Sm_{CN} and Nb/Ta ratios (Fig.

7 and Electronic Supplement 2). The Cr content directly reflects the few percent of disseminated chromite in dunites, which also seems to control the whole rock Zr/Hf ratio (Electronic Supplement 2).

The most impressive mineral composition variations along the three cross-sections are observed in pure dunites or more generally at the base of each section below the N155-170 fault (Fig. 6). They are unpredictable as they are not related to the samples modal composition. Conversely, Fo in olivine (100 × molar $Mg/(Mg + Fe_{total})$), XCr in chromite (100 × molar Cr/(Cr + Al)) (Fig. 6) and Mg# in whole rock (100 × molar $Mg/(Mg + Fe_{total})$) (Fig. 7) are much less variable in impregnated dunites, whatever the nature of interstitial minerals.

3.3.2. Chemical trends related to fault zones

In some cases, especially in pure dunites, the vertical evolution of chemical signatures along the cross-sections define patterns that appear to be influenced by the distribution of major fault zones, whatever their orientation. In details, the Fo in olivine, XCr in chromite and Mg# in whole rock decrease down to values of about 88 or below, ~45 and ~87 respectively approaching faults (e.g. the interval ~700-725 m in the three sections; Figs. 5 and 6). NiO in olivine and Ni in whole rock follow the same tendency as well as the Mg# (100 × molar $Mg/(Mg + Fe^{2+})$) in clinopyroxene, orthopyroxene and amphibole, both when they are interstitial between olivine grains or as inclusions in chromite (Electronic Supplement 2). The La_{CN}/Sm_{CN} and U/Th ratios in pure dunites also decrease until 1 and below 0.75 respectively (toward 700 m and 775 m in altitude in the cross-section #1, 725 m and 850 m in the cross-section #3; Fig. 7). These variations are correlated with an increase of the CaO content in olivine in pure dunites (until ~0.3 wt.%), TiO_2 content in pyroxenes (up to 0.5 wt.%) (Fig. 6

and Electronic Supplement 2). Similarly, Gd_{CN}/Yb_{CN} (and thus the concavity of the REE patterns) and Nb/Ta ratios in whole rocks increase in pure dunites toward most of the fault zones (Fig. 7 and Electronic Supplement 2).

3.3.3. Chemical trends unrelated to lithological or structural features

Beyond variations related to the amount of interstitial phases (local-scale) or approaching fault zones (tens of meter-scale), we can observe chemical evolutions depending on the altitude along the whole DTZ. In this frame, Mg# and Ni content in both whole rock and minerals generally decrease in the uppermost part of the DTZ. In the same time TiO_2 content in ortho- and clinopyroxene and Na_2O content in amphibole increase whatever their mode of occurrence (i.e. interstitial between olivine grains or included in chromite). This suggests that DTZ dunites recorded the cumulate effect of several processes involved in their formation. Concerning few chemical proxies, such as Co in whole rock or YFe^{3+} in chromite, their vertical evolution is partly correlated to the presence of fault zones but without clear systematic increasing or decreasing trend (Electronic Supplement 2). This leads to the alternation of positive and negative correlations between Ni and Co in some horizons like at the base of the cross-section #1.

3.3.4. Focus on clinopyroxene major element zoning

It was shown in previous studies that chemical zonings in interstitial minerals in deeply impregnated mantle-derived rocks probably reflect melt/rock reactions (e.g. Drouin et al., 2009; Sanfilippo et al., 2015). Among the studied impregnated samples, twenty chemical profiles were performed across single grains of clinopyroxene in order to investigate the pattern of possible zoning in their major element composition as it was already reported (even if not systematic) in some cases (Koga et al., 2001; Rospabé et al., 2018a). This was made for

clinopyroxene of various sizes in 11 samples displaying various interstitial minerals in variable amount. Half of the analyzed clinopyroxene shows an increase in Mg# (up to 92.5), and in SiO_2 and TiO_2 contents (up to 53.8 wt.% and 0.33 wt.% respectively), associated to a decrease of Al_2O_3 and Cr_2O_3 contents (down to 2.8 wt.% and 1.2 wt.% respectively), from core to rims (Fig. 8A). The other half does not show zoning in Mg# and SiO_2, and show normal zoning in Al_2O_3 and Cr_2O_3 in some cases only (Fig. 8B). It appears that both the chemical content of and the presence/absence of zoning in clinopyroxene are independent of the paragenetic assemblage, neither with the degree of impregnation nor with the size of the considered clinopyroxene crystal. However, well-defined zonings are systematically observed in samples collected close to fault zones. Oppositely, chemically weakly zoned clinopyroxenes are observed in samples located everywhere in the DTZ, independently from any fault location.

4. Interpretations and discussion

4.1. Early syn-magmatic faulting at Moho level

The faults located between the distinctive main units of the Sumail massif were originally attributed to later tectonic events postdating the oceanic lithosphere accretion, potentially related to the emplacement of the ophiolitic nappe onto the Arabian margin (Amri, 1995; Glennie et al., 1974; Rabu et al., 1986). Other studies interpreted the development of the both N130 and N165 tectonic systems as synchronous with magmatism, these features being responsible for the deformation and disturbed crystallization in the lower crustal, layered gabbros along N130 faults (Abily et al., 2011; Jousselin et al., 1998), and of the genesis of plagiogranitic and andesitic intrusions within the N165-trending Muqbariah regional shear zone system (Amri et al., 1996; Benoit et al., 1999).

We observed that the DTZ was also affected by the both N130 and N165-180 systems (Fig. 1B), which led to a stronger serpentinization and carbonation of surrounding dunites. In spite of these ubiquitous witnesses of low temperature hydrothermal circulations, some outcrops preserved strong evidence of a high temperature deformation of the magmatic products along the both fault systems (Figs. 2A and B). Excepting the two main N165-180 discontinuities, which accommodated a significant strike-slip displacement (i.e. estimated to 80 m horizontally concerning the easternmost one), other faults are better described as cracks with a movement restricted to a few meters at most. The N130-trending faults may reasonably be related to the ridge accretion, the strike of the sheeted dike complex displaying the same orientation in this area (MacLeod and Rothery, 1992; Pallister, 1981). The slight normal displacement on fault planes, generally measured with a dip of 50 to 70° at a regional scale, locally induced the syn-magmatic deformation and the disturbance of crystallization sequences in layered troctolites and gabbros at the transition between the crustal section and the DTZ (Fig. 2A; see also Abily and Ceuleneer, 2011). The two areas affected by N130 faults with an opposite dipping toward the SW (along the cross-section #2) define local graben-type structures accommodating the general extensional frame (Fig. 1B). We observed that N130 oriented mafic dikes, viewed as cumulates after the last basaltic melt batches discharged from the Maqsad diapir (Ceuleneer et al., 1996), cut across the tectonic lineaments, especially the transtensional N165 ones (Fig. 2C). This supports that most of the N130 and N165 tectonic events on one hand and the magmatic activity on the other hand developed then ceased contemporaneously.

Otherwise, chemical variations observed vertically along the DTZ constitute an independent and indirect argument supporting syn-magmatic fluid circulation along faults that experienced moderate displacement. The minerals (both olivine and impregnating phases) and bulk-rock

401 display evolutions of their composition over tens of meters vertically toward the fault zones,
402 including for immobile elements or element ratios, expected to be related to magmatic
403 processes only (e.g. XCr in chromite, TiO_2 in impregnant minerals or REE and HFSE in bulk-
404 samples; Figs. 5 and 6, Electronic Supplement 2). Such continuous evolutions suggest that
405 faults played an important role in the DTZ genesis and are consistent with a moderate
406 amplitude of the displacements along fault planes: major offsets post-dating the DTZ
407 formation would have partly erased the systematic chemical trends observed approaching the
408 faults. It is worth mentioning that common vertical chemical evolutions are observed both in
409 minerals composing dunites as well as in silicate inclusions, supposed to be isolated early by
410 their host chromite. Consequently, all these observations allow us to interpret both N130 and
411 N165 oriented faults as structures developed early at a high temperature, syn-magmatic stage.
412 They strongly influenced the petrological and geochemical organization of the DTZ, although
413 they continued to be main vectors for hydrothermal fluids at lower temperature, following the
414 cessation of any magmatic activity.
415
416 *4.2. Relationships between faulting and melt-rock reactions*
417 *4.2.1. Faulting and percolating melts characteristics*
418 The relationship between fault zones and minerals/whole rock compositions designs several
419 similar chemical evolutions along the three cross-sections - especially between cross-sections
420 #1 and #3 that also display a similar petrological sequence (Fig. 3). Fault zones partly
421 condition the chemical patterns recorded in the dunitic matrix as revealed by olivine and pure
422 dunites whole rock compositions. The decrease of Fo in olivine and La_{CN}/Sm_{CN} ratio
423 associated to an increase of the CaO content in olivine and Gd_{CN}/Yb_{CN} ratio in pure dunites
424 (Figs. 6 and 7) was previously attributed to the percolation of MORB and subsequent
425 reequilibration with the surrounding olivine (Abily and Ceuleneer, 2013; Rospabé et al.,

2018a). This implies the overprint of a MORB signature over a prior enriched signature potentially related to the genesis of small melt batches enriched in H_2O, silica and incompatible trace elements during the early dunitization (Rospabé et al., 2018a). This interpretation is also supported by the fractionation of U/Th and Nb/Ta ratios from the dunitic horizons toward fault zones (decrease of U/Th and increase of Nb/Ta toward faults with few exceptions; Fig. 7), considering that U is known to be a fluid/hydrous melt mobile element and Ta is likewise expected to be much more easily mobilized by hydrous fluids or melts than by dry (or slightly hydrated) melt - MORB in our case - relative to Nb (Green, 1995). Evolutions of the chemical composition of the dunitic matrix, as well as of impregnant minerals (chromite, clinopyroxene, orthopyroxene and amphibole) at the approach of fault zones indicates that syn-magmatic faults conditioned the nature of the melt that circulated through the DTZ. A reasonable way to account for these observations is to envision a hybridization process between different melt batches within fault zones, which hence leads to an evolving reequilibration signature within the host olivine matrix, i.e. starting from faults and propagating into the surrounding dunitic horizons.

The introduction of hydrous fluids into the DTZ from above at an early magmatic stage is strongly supported by the petrological sequences along both cross-sections #1 and #3: interstitial orthopyroxene and amphibole appear in the shallowest levels of the DTZ, just above fault zones (N130 in the case of cross-section #1, N155 in the case of cross-section #3). This observation was previously attributed to the hybridization of upwelling MORB with downwelling hydrothermal fluids and/or hydrated silica-rich melts issued from the hydrous melting of surrounding rocks, with an increase of the hydrothermal component upsection (Rospabé et al., 2017). The correlation between syn-magmatic faults (see paragraph 4.1) and the appearance of minerals indicative of a hydrated magmatic environment supports that the

DTZ was continuously hydrated all along its development thanks to fracturing, from the prior dunitization stage until the later stage when more and more percolating melts invaded the DTZ. Finally, along fault zones occurs the hybridization between (1) the first interstitial H_2O- and silica-rich melts batches, (2) MORB issued from the deeper mantle partial melting and drained along faults through the DTZ, and (3) possibly continuous supply of hydrothermal fluids. The low Nb/Ta ratios within pure dunitic horizons (Fig. 7) may reflect melt-rock reaction at low melt/rock ratio (see Kelemen et al. (1993) concerning arc magmas generation and evolution, and Rospabé et al. (2018) concerning the present Maqsad DTZ), and/or that the early hydrated, enriched melt has fractionated a small amount of hydrous and Ti-rich minerals such as amphibole or mica (Bodinier et al., 1996; Green, 1995) prior to the reequilibration with the surrounding dunitic matrix. This later hypothesis is in accordance with (1) the assumption that this exotic melt was involved in the transport and the widespread fractionation of chromite at Moho level, chromite that entrapped inclusions of amphibole and mica (Rospabé et al., 2017; 2018), and (2) the observation of an increasing amount of chromite, especially as schlierens, approaching the faults (Figs. 3 and 4B; see also the vertical evolution of Cr in whole rock in the Electronic Supplement 2). It is worth noting that pure dunites that present a quite high Nb/Ta ratio while being located few tens of meters far from fault zones, chiefly at the base of the cross-section #1 (Fig. 7), generally correspond to samples containing schlierens of chromite (see the correspondence between the whole rock Cr content and HFSE ratios in the Electronic Supplement 2) that contain Ti-rich mineral inclusions. At a much larger scale, chromitite deposits were regularly observed along major shear zones within the DTZ and the uppermost part of the mantle section of the Oman ophiolite (Boudier and Al-Rajhi, 2014; Zagrtdenov et al., 2018).

4.2.2. Faulting and refertilization

476 Accordingly, the fact that the cross-section #2, in intermediate location between sections #1
477 and #3 (Figs. 1B and 3), is more impregnated all the way up may be related to its peculiar
478 structural situation. A large part of this section is enclosed in a graben structure, bordered by
479 N130 fault zones with an opposite dip. Accordingly, we interpret this location as a main
480 avenue for melt percolation, issued from the mantle partial melting, and for hydrothermal
481 fluids circulation, introduced along fault zones. This led to strong fluid-melt-rock reactions
482 and to the refertilization of the dunitic matrix, potentially linked to a temperature decrease
483 within the graben structure. Contrariwise, pure dunitic horizons in sections 1 and 3 were
484 compacted at higher temperature before massive crystallization from interstitial melts.
485
486 Clinopyroxene grains from samples collected few meters from faults preserve a chemical
487 zoning while zoning is uncommon at larger distance (Fig. 8A). The occurrence or absence of
488 zoning is unrelated to the modal composition of the rock and from the grain size and seems to
489 depend only on the vicinity of a fault. Such chemical zonings in strongly impregnated
490 peridotites (frequently described as “olivine-rich troctolites”) collected along detachment
491 faults in present-day ridges and in ophiolites were previously interpreted as the result of
492 reactive crystallization (e.g. Drouin et al., 2009; Sanfilippo et al., 2015 and references
493 therein), i.e. mineral fractionation associated to harzburgite orthopyroxene or dunite olivine
494 assimilation (Collier and Kelemen, 2010). The importance of reactive crystallization relative
495 to fractional crystallization was previously considered as limited in the case of the Maqsad
496 DTZ (Rospabé et al., 2018a). Nonetheless, our results allow us to consider that, even if the
497 refertilization process was dominated by fractional crystallization from percolating melts, the
498 development of syn-magmatic fault zones during the DTZ formation reinforced local (fluid-
499)melt-rock reactions triggering reactive crystallization. Therefore, we propose that strong
500 relationships between the structural environment and mantle refertilization may be the key to

501 decipher the origin of hybrid olivine-rich troctolites along oceanic core complex (Sanfilippo
502 et al., 2015 and references therein).
503
504 *4.3. Implications for the development of the DTZ and melt migration beneath spreading*
505 *centres*
506 The progressive chemical evolution vertically along the DTZ, starting from a enriched melt
507 and acquiring progressively a MORB signature, reflects that the hybridization between
508 different melt batches is enhanced in fault zones that are avenues for both melt and fluids
509 circulations. The syn-magmatic faults affecting the DTZ, whatever their orientation but with a
510 dipping frequently higher than 60°, may have assisted the MORB extraction from the Maqsad
511 diapir. In this way, the most salient MORB signature is markedly recorded in dunites located
512 close to N165-N180 fault zones (e.g. higher CaO values; Fig. 6), the percolation having
513 potentially been facilitated by the transtensional feature. Moreover, troctolite intrusions
514 observed in the highest levels of the DTZ might represent the last extracted melt batches,
515 which suffered fractional crystallization due to cooling. In other words, it appears that the
516 DTZ recorded the switch between different melt extraction modes, starting with pervasive
517 porous flow within the host dunite (strongest MORB-reequilibrated signature at the approach
518 of faults), then followed in time when temperature decreases by melt discharges focused
519 along fault zones (cumulate troctolite intrusions). In Figure 9 we propose a synthetic scenario
520 for the DTZ formation above the Maqsad diapir:
521 - Stage A: Fault zones (important dipping, slight displacement) affect the DTZ early.
522 They allow the introduction of fluids at Moho level that potentially assist the orthopyroxene
523 melting out, leading to the mantle harzburgite transformation into dunite (Rospabé et al.,
524 2017), and to the early generation of small volume of H_2O-, SiO_2 and incompatible trace
525 elements enriched melts (Rospabé et al., 2018a).

- Stages B and C: Subsequently, fault zones focus the percolation of MORB issued from the continuous partial melting of mantle peridotites, allowing (1) to a more or less strong chemical reequilibration with host dunite, (2) to their hybridization with prior enriched melt which has a direct influence on the Cr redistribution at Moho level, (3) to their accumulation at certain levels, and (4) to the refertilization of the host dunite, mainly to the top of the DTZ, with anhydrous or hydrated minerals fractionation interstitially (fractional or reactive crystallization).

-Stage D: In addition to their strong influence on fluid-melt-rock reactions at Moho level, fault zones drain residual melts from the DTZ to the lower crust. Plurimetric intrusions of cumulate troctolites, becoming more and more abundant in the uppermost DTZ, are witnesses of these melt discharges before/during the magmatic activity cessation.

Beyond the structural control on the magmatic processes that occur within the oceanic Moho, fault zones continued to focus fluid circulation at lower temperature after the cessation of the magmatic activity. In addition to the Cr transport at high temperature and its massive fractionation as chromitite ore bodies that may have occurred preferentially along fault zones (Boudier and Al Rajhi, 2014; Zagrtdenov et al., 2018), later hydrothermal circulations along long-standing fractures should have led to strong chemical exchanges during low temperature alteration of the lower crust (Zihlmann et al., 2018) and serpentinization and carbonation at Moho level.

5. Conclusion

The fluid-melt-rocks reactions occurring at the mantle-crust transition below oceanic spreading centers are expected to significantly influence the nature of the melts that feed the crust and the chemical exchanges between the deep lithosphere and superficial envelopes. Our

551 combined structural, petrological and geochemical study of the DTZ in the Sumail massif
552 reveals that syn-magmatic tectonic lineaments primarily control these reactions. The Maqsad
553 DTZ evolved in a transtensional environment induced by two N130 and N165-180 fault
554 systems related to the complex (asymmetric) oceanic accretion geometry. Surprisingly, both
555 systems seem to have influenced the petrological and geochemical organization of the DTZ,
556 supporting their contemporaneity as formulated on the basis of field evidence. They both
557 govern:
558 (1) the vertical chemical evolutions recorded in the olivine matrix and the interstitial minerals
559 over tens of meters approaching faults zones, concerning elements considered immobile in
560 fluids or during alteration such as REE, HFSE or Th (i.e. reflecting the overprint of several
561 processes: the prior dunitization process, the focused migration of interstitial melts and/or
562 fluids through the dunitic matrix along fault zones, and the modification of the percolating
563 melt chemistry by hybridization);
564 (2) the petrological organization of the DTZ (i.e. the succession of pure and impregnated
565 horizons, that reflects the spatial distribution of melt crystallization products).
566 In this frame, the fact that faults affect syn-magmatically the mantle-crust transition zone may
567 be considered as the missing link between high temperature magmatic-related chemical
568 imprints in DTZ dunites, the evident involvement of a hydrous component, the migration and
569 extraction of percolating melts, and the mobilization and precipitation of a high amount of Cr
570 within this interface. Moreover, the successive melt discharges from the DTZ to the crust,
571 following different extraction modes, may have potentially contributed to the heterogeneity
572 observed in the Oman ophiolite crust (Jansen et al., 2018) and along oceanic spreading centers
573 worldwide.
574 Finally, syn-magmatic faults may have a great effect on the thermal and rheological structure
575 of the oceanic lithosphere while they also apparently strongly influence chemical

geodynamics (metals, sulfur and carbon cycles and so on) in oceanic ridges environment since fluids are introduced continuously along fault zones, from (more or less hydrated) magmatic stage to later, low temperature serpentinization and carbonation related to solely seawater-derived hydrothermal circulations. These findings may contribute to better understand the connection between the petrological, chemical and alteration reactions at Moho level and within the lower oceanic crust, and the thermal, tectonic and rheological structure of the whole oceanic lithosphere.

Acknowledgments

We would like to thank F. de Parseval, J.-F. Ména and L. Menjot for thin sections preparation and, for technical assistance during sample preparation and data acquisition, M. Henry and Jonathan Prunier (cleanroom lab), S. Gouy, J. Langlade and Ph. de Parseval (microprobe analysis), F. Candaudap (HR-ICP-MS for whole rock trace elements analysis) and D. Roggero (LA-ICP-MS for clinopyroxene trace elements analysis). We are grateful to H. Al Azri for its hospitality, as well as to M. Al Araimi, M. Al Batashi, A. Al-Rajhi, S. Almusharrafi and other colleagues from the Ministry of Commerce and Industry, Sultanate of Oman, for their kind support. We greatly thank A. Sanfilippo and an anonymous reviewer for their constructive comments, as well as T. A. Mather for editorial handling and comments, which helped to improve this manuscript. This work has benefited from a financial support provided by the Centre National de la Recherche Scientifique-Institut National des Sciences de l'Univers (CNRS-INSU).

Figure 1. (A) Simplified geological map of the Sumail massif (modified after Béchennec et al. (1992) and Wyns et al. (1992)). The massif exposes a N130-oriented paleo-ridge spreading centre. It is centred on a mantle paleo-diapir structure defined by the vertical mantle flow

601 structure observed in the Maqsad area (Ceuleneer et al., 1988; Jousselin et al., 1998). The
602 dunitic transition zone is well exposed along the ridge axis and to the SW between the ridge
603 axis and the N165 ductile Muqbariah fault system. The white rectangle highlights our study
604 area. (B) Detailed geological map of the studied area (modified after Rabu et al. (1986)). The
605 dunitic transition zone (DTZ) is more than 300 m thick along the ridge axis. The three studied
606 cross-sections (cross-sections #1, #2 and #3 from north to south) were sampled from the wadi
607 Mahram to the west to the higher levels of the DTZ to the east. The sampling density we
608 adopted (step of 10 to 20 meters of elevation) has been previously shown to be optimal to the
609 description of the vertical petrological and geochemical variability through the DTZ (Abily
610 and Ceuleneer, 2013; Rospabé, 2018), particularly in the Sumail massif where the paleo-
611 Moho is sub-horizontal with a weak ESE regional dip (i.e. current absolute altitudes
612 correspond closely to paleo-depth). Structural measurements completed during our field
613 exploration are also reported on this sketch, especially the dipping and the dipping direction
614 along the two N130 and N165-N180 main fault systems identified in this area. The along
615 strike extent of the main faults exceeds several kilometers.
616
617 **Figure 2.** Three examples of relationships between deformed magmatic features and N130
618 (A) or N165-180 (B and C) fault zones affecting the DTZ in the studied area. A) A layered
619 troctolite lens is offset by about few meters along a N130.70NE normal fault making the
620 contact with surrounding dunite (left). These mafic cumulates recorded a strong deformation
621 near the fault plane (centre) while plagioclases show a remarkable elongation within the
622 groundmass (right). B) Deformation of magmatic products in the tectonic corridor located at
623 the base of the studied cross-sections and separating the DTZ from the harzburgite mantle
624 section (Fig. 1B). Among others, we observed an elongated gabbroic boudin (top) or flames
625 structures displayed by gabbros laminated within the host dunite (centre) along the N180.80W

626 fault, as well as aligned and elongated plagioclase impregnations in dunites (bottom) along
627 the N165.85E major fault. C) A N165.80W fault zone cross-cutting the cross-section #1 is
628 characterized by a well organized schistose parting in dunites (left) with no evidence of
629 mylonitic deformation (right top). An undeformed amphibole-bearing gabbroic dike, oriented
630 N125.70NE, cross-cut the schistosity of the N165.80W fault zone (right bottom).
631
632 **Figure 3.** Petrological and structural logs of the three studied cross-sections: from north to
633 south the section #1 (293 m), the section #2 (343 m) and the section #3 (371 m). Regardless
634 of the petrological sequences of the DTZ - a lower pure dunitic half surmounted by an
635 impregnated half (cross-sections #1 and #3), or more extensively impregnated (cross-section
636 #2) -, the transition from a lithological facies to another generally corresponds to the presence
637 of a fault zone. There is no systematics between the direction of the fault, N130 or N165-180,
638 and the minerals distribution.
639
640 **Figure 4.** Photomicrographs showing the different mineral contents characterizing the DTZ
641 dunites in the Maqsad area, with A) a “pure dunite”, almost made of olivine and chromite
642 only and containing a very few amount (<0.5%) of small (few hundreds microns at most)
643 clinopyroxene rims between two olivine grains or located at 120° olivine grains triple
644 junctions (16OM07A - cross-section #3), B) a dunite containing chromite organized as
645 schlierens (16OM24A - cross-section #3), C) an orthopyroxene oikocryst in an opx/pl/cpx-
646 bearing dunite (16OM29 - cross-section #3), D) a part of a clinopyroxene oikocryst up to 5
647 mm in a strongly impregnated pl/cpx-bearing dunite (16OM49 - cross-section #2), and E)
648 interstitial amphibole in an amph-bearing dunite (± opx/pl/cpx) (16OM74B - cross-section
649 #2).
650

Figure 5. Chemical variations along cross-sections 1, 2 and 3 in the Maqsad dunitic transition zone (data for cross-section 1 are from Rospabé et al. (2018), data for cross-sections 2 and 3 are newly presented here). A) NiO content as a function of Fo in olivine, B) whole rock chondrite-normalized REE and Primitive Mantle-normalized multi-elements patterns of pure dunites (in the middle) and impregnated dunites (at the bottom). The precision is better than 10% for LILE, REE, Pb, Th and U, and better than 20% for HFSE (see also Rospabé et al., 2018b). Grey fields represent the entire variation ranges described in Rospabé et al. (2018). Analytical methods used to acquire the data are detailed in the Electronic Supplement 1. Chondrite and Primitive Mantle normalizing values are from Barrat et al. (2012) and Sun and McDonough (1989) respectively.

Figure 6. Vertical evolution of the mineral chemical composition along the studied cross-sections, plotted as a function of the altitude. The colours of the dots represent the different lithological facies, with pure dunites in blue, cpx-bearing dunites in red, pl/cpx-bearing in orange, opx/pl/cpx-bearing dunite in purple and amph-bearing dunites in green. Red dashed lines are faults, each being localized where they respectively cut across each section. The grey gradient highlights the vertical increasing or decreasing characteristic of each element or element ratio, in some case related to the presence of fault zones. Are represented the Fo (100 × molar $Mg/(Mg + Fe_{total})$) and the CaO content (wt.%) in olivine, the XCr (100 × molar $Cr/(Cr + Al)$) in chromite and the TiO_2 content (wt.%) in clinopyroxene. Mineral compositions for samples from the cross-section #1 are issued from Rospabé et al. (2018), corresponding to the "Buri cross-section". The amount of impregnation is also reported to the left as a function of the altitude. The modal content, available in Supplementary Table 1, was calculated using the MINSQ least squares method (Herrmann and Berry, 2002) based on whole rock and minerals major element compositions.

Figure 7. Vertical evolution of the whole rock chemical composition along the studied cross-sections, plotted as a function of the altitude. The colours of the dots represent the different lithological facies, with pure dunites in blue, cpx-bearing dunites in red, pl/cpx-bearing in orange, opx/pl/cpx-bearing dunite in purple and amph-bearing dunites in green. Red dashed lines are faults, each being localized where they respectively cut across each section. The grey gradient highlights the vertical increasing or decreasing characteristic of each element or element ratio, in some case related to the presence of fault zones. Are represented the Mg# (100 × molar Mg/(Mg + Fe_{total})), La_{CN}/Sm_{CN}, Nb/Ta and U/Th ratios. Chondrite normalizing values used to calculate the La_{CN}/Sm_{CN} ratio are from Barrat et al. (2012). Whole rock compositions for samples from the cross-section #1 are issued from Rospabé et al. (2018), corresponding to the "Buri cross-section". The amount of impregnation is also reported to the left as a function of the altitude. The modal content, available in Supplementary Table 1, was calculated using the MINSQ least squares method (Herrmann and Berry, 2002) based on whole rock and minerals major element compositions.

Figure 8. Magnesium number (Mg# = 100 × molar Mg/(Mg + Fe^{2+})) and SiO_2, Al_2O_3, Cr_2O_3 and TiO_2 concentration profile across two clinopyroxenes from opx/pl/cpx-bearing dunites (15OM03A to the left, 16OM26 to the right). A) The first one to the left shows a well-defined composition zoning with an increase of Mg# and SiO_2 and TiO_2 contents, together with the decrease of Al_2O_3 and Cr_2O_3, from core to rims. This pattern is similar to what is observed in the case of reactive crystallization in abyssal olivine-rich troctolites, when the surrounding peridotite is partly assimilated during fractional crystallization (Sanfilippo et al., 2015 and reference therein). B) The second one to the right exhibits patterns more random in Mg#, flattest in SiO_2 and TiO_2, and similar to the first one in Al_2O_3 and Cr_2O_3 with the same

701 decrease toward grain rims.

702

703 **Figure 9.** Synthetic model for the DTZ vertical structuration in the Maqsad area. Stage A:
704 Introduction of fluids at Moho level along fault zones which potentially assist the upper
705 mantle dunitization (Rospabé et al., 2017) and, consequently, leads to the generation of small
706 melts batches enriched in H_2O-, SiO_2 and incompatible trace elements (Rospabé et al.,
707 2018a). Stage B: Ascending MORB percolation focused along fault zones, hybridization
708 between MORB and the early interstitial enriched melt, reequilibration with the surrounding
709 dunitic matrix, melt accumulation and interstitial mineral crystallization in the upper levels of
710 the DTZ (fractional or reactive crystallization depending on the distance to faults). Stage C:
711 Fractionation of hydrous minerals, or anhydrous minerals witnessing of hydrous melts
712 percolation, following the continuous hybridization between MORB and other exotic melts
713 through the DTZ. This hybrid melt is involved in the mobilization and precipitation of Cr.
714 Note that stages B and C may be contemporaneous since it has been evidenced that exotic
715 H_2O- and SiO_2-rich melt were involved as early as the dunitization itself (Rospabé et al.,
716 2017; 2018). The two stages were here decoupled to make easier the understanding of the
717 structural, petrological and geochemical organization of the DTZ. Stage D: Residual melts
718 extraction from the DTZ to the crust, with the formation of entrapment zones represented by
719 cumulate troctolite intrusions at the top of the DTZ. Subsequent alteration (serpentinization,
720 carbonation) of the DTZ dunites, especially along faults and fractures, follows the magmatic
721 activity cessation.

722

723 **References**

724 Abily, B., Ceuleneer, G., 2013. The dunitic mantle-crust transition zone in the Oman
725 ophiolite: Residue of melt-rock interaction, cumulates from high-MgO melts, or both?

Geology 41, 67-70. doi:10.1130/G33351.1

Abily, B., Ceuleneer, G., Launeau, P., 2011. Synmagmatic normal faulting in the lower oceanic crust: Evidence from the Oman ophiolite. Geology 39, 391-394. doi:10.1130/G31652.1

Akizawa, N., Arai, S., Tamura, A., Uesugi, J., Python, M., 2011. Crustal diopsidites from the northern Oman ophiolite: Evidence for hydrothermal circulation through suboceanic Moho. J. Mineral. Petrol. Sci. 106, 261-266. doi:10.2465/jmps.110621b

Amri, I., 1995. Etude pétrologique et structurale d'une dorsale océanique fossile, Massif de Sumail (ophiolite d'Oman). Implications pour les mécanismes d'accrétion océanique. Université Paul Sabatier, Toulouse III.

Amri, I., Benoit, M., Ceuleneer, G., 1996. Tectonic setting for the genesis of oceanic plagiogranites: evidence from a paleo-spreading structure in the Oman ophiolite. Earth Planet. Sci. Lett. 139, 177-194. doi:10.1016/0012-821X(95)00233-3

Barrat, J.-A., Zanda, B., Moynier, F., Bollinger, C., Liorzou, C., Bayon, G., 2012. Geochemistry of CI chondrites: Major and trace elements, and Cu and Zn Isotopes. Geochim. Cosmochim. Acta 83, 79-92. doi:10.1016/j.gca.2011.12.011

Béchennec, F., Roger, J., Le Métour, J., Wyns, R., 1992. Geological Map of Seeb: Sheet NF 40-03, Scale: 1:250,000. Explanatory Notes. Dir. Gen. Miner. Oman Minist. Pet. Miner.

Benoit, M., Ceuleneer, G., Polvé, M., 1999. The remelting of hydrothermally altered peridotite at mid-ocean ridges by intruding mantle diapirs. Nature 402, 514-518. doi:10.1038/990073

Benoit, M., Polvé, M., Ceuleneer, G., 1996. Trace element and isotopic characterization of mafic cumulates in a fossil mantle diapir (Oman ophiolite). Chem. Geol. 134, 199-214. doi:10.1016/S0009-2541(96)00087-3

Bodinier, J.L., Merlet, C., Bedini, R.M., Simien, F., Remaidi, M., Garrido, C.J., 1996.

751 Distribution of niobium, tantalum, and other highly incompatible trace elements in the
752 lithospheric mantle: The spinel paradox. Geochim. Cosmochim. Acta 60, 545-550.
753 doi:10.1016/0016-7037(95)00431-9
754 Bosch, D., Jamais, M., Boudier, F., Nicolas, A., Dautria, J.M., Agrinier, P., 2004. Deep and
755 high-temperature hydrothermal circulation in the Oman ophiolite-petrological and
756 isotopic evidence. J. Petrol. 45, 1181-1208. doi:10.1093/petrology/egh010
757 Boudier, F., Al-Rajhi, A., 2014. Structural control on chromitite deposits in ophiolites: the
758 Oman case. Geol. Soc. London, Spec. Publ. 392, 263-277. doi:10.1144/SP392.14
759 Boudier, F., Ceuleneer, G., Nicolas, A., 1988. Shear zones, thrusts and related magmatism in
760 the Oman ophiolite: Initiation of thrusting on an oceanic ridge. Tectonophysics 151, 275-
761 296. doi:10.1016/0040-1951(88)90249-1
762 Boudier, F., Nicolas, A., 1995. Nature of the moho transition zone in the Oman ophiolite. J.
763 Petrol. 36, 777-796. doi:10.1093/petrology/36.3.777
764 Ceuleneer, G., 1991. Evidence for a Paleo-Spreading Center in the Oman Ophiolite: Mantle
765 Structures in the Maqsad Area. Springer Netherlands, pp. 147-173. doi:10.1007/978-94-
766 011-3358-6_9
767 Ceuleneer, G., Le Sueur, E., 2008. The Trinity ophiolite (California): the strange association
768 of fertile mantle peridotite with ultra-depleted crustal cumulates. Bull. Soc. Géol. Fr.
769 179, 503-518. doi:10.2113/gssgfbull.179.5.503
770 Ceuleneer, G., Monnereau, M., Amri, I., 1996. Thermal structure of a fossil mantle diapir
771 inferred from the distribution of mafic cumulates. Nature 379, 149-153.
772 doi:10.1038/379149a0
773 Ceuleneer, G., Nicolas, A., 1985. Structures in podiform chromite from the Maqsad district
774 (Sumail ophiolite, Oman). Miner. Depos. 20, 177-184. doi:10.1007/BF00204562
775 Ceuleneer, G., Nicolas, A., Boudier, F., 1988. Mantle flow pattern at an oceanic spreading

776 centre: the Oman peridotite record. Tectonophysics 151, 1-26. doi:10.1016/0040-
777 1951(88)90238-7
778 Clénet, H., Ceuleneer, G., Pinet, P., Abily, B., Daydou, Y., Harris, E., Amri, I., Dantas, C.,
779 2010. Thick sections of layered ultramafic cumulates in the Oman ophiolite revealed by
780 an airborne hyperspectral survey: Petrogenesis and relationship to mantle diapirism.
781 Lithos 114, 265-281. doi:10.1016/j.lithos.2009.09.002
782 Collier, M. L., Kelemen, P. B., 2010. The case for reactive crystallization at mid-ocean ridges.
783 J. Petrol. 51, 1913-1940. doi:10.1093/petrology/egq043
784 Currin, A., Wolff, P. E., Koepke, J., Almeev, R. R., Zhang, C., Zihlmann, B., Ildefonse, B.,
785 Teagle, D. A., 2018. Chlorine-rich amphibole in deep layered gabbros as evidence for
786 brine/rock interaction in the lower oceanic crust: A case study from the Wadi Wariyah,
787 Samail Ophiolite, Sultanate of Oman. Lithos 323, 125-136.
788 doi:10.1016/j.lithos.2018.09.015
789 Drouin, M., Godard, M., Ildefonse, B., Bruguier, O., Garrido, C.J., 2009. Geochemical and
790 petrographic evidence for magmatic impregnation in the oceanic lithosphere at Atlantis
791 Massif, Mid-Atlantic Ridge (IODP Hole U1309D, 30°N). Chem. Geol. 264, 71-88.
792 doi:10.1016/j.chemgeo.2009.02.013
793 France L., Ildefonse B., Koepke J., 2013. Hydrous magmatism triggered by assimilation of
794 hydrothermally altered rocks in fossil oceanic crust (northern Oman ophiolite).
795 Geochem. Geophys. Geosyst., 14, 2598-2614. doi:10.1002/ggge.20137
796 France L., Ildefonse B., Koepke J., 2009. Interactions between magma and hydrothermal
797 system in Oman ophiolite and in IODP Hole 1256D: fossilization of a dynamic melt lens
798 at fast spreading ridges. Geochem. Geophys. Geosyst., 10, Q10019. doi:
799 10.1029/2009GC002652
800 Gente, P., Pockalny, R. A., Durand, C., Deplus, C., Maia, M., Ceuleneer, G., Mével, C,

Cannat, M, Laverne, C., 1995. Characteristics and evolution of the segmentation of the Mid-Atlantic Ridge between 20°N and 24°N during the last 10 million years. Earth Planet. Sci. Lett. 129, 55-71. doi:10.1016/0012-821X(94)00233-O

German, C.R., Petersen, S., Hannington, M.D., 2016. Hydrothermal exploration of mid-ocean ridges: Where might the largest sulfide deposits be forming? Chem. Geol. 420, 114-126. doi:10.1016/j.chemgeo.2015.11.006

Gilgen S.A., Diamond L.W., Mercolli I., 2016. Sub-seafloor alteration: Timing, depth and stratigraphic distribution in the Semail ophiolite, Oman. Lithos, 260, 191-210. doi: 10.1016/j.lithos.2016.05.014

Glennie, K.W., Boeuf, M.G.A., Hughes Clarke, M.W., Moody-Stuart, M., Pilaar, W.F.H., Reinhardt, B.M., 1974. Geology of the Oman Mountains. Verh. van het K. Ned. Geol. Mijnbouwkd. Genoot. 31, 423 pp.

Green, T.H., 1995. Significance of Nb/Ta as an indicator of geochemical processes in the crust-mantle system. Chem. Geol. 120, 347-359. doi:10.1016/0009-2541(94)00145-X

Gregory, R.T., Taylor, H.P., 1981. An oxygen isotope profile in a section of Cretaceous oceanic crust, Samail Ophiolite, Oman: Evidence for δ18O buffering of the oceans by deep (>5 km) seawater-hydrothermal circulation at mid-ocean ridges. J. Geophys. Res. Solid Earth 86, 2737-2755. doi:10.1029/JB086iB04p02737

Herrmann, W., Berry, R. F., 2002. MINSQ - a least squares spreadsheet method for calculating mineral proportions from whole rock major element analyses. Geochemistry Explor. Environ. Anal. 2, 361-368. doi:10.1144/1467-787302-010

Jansen, M. N., Lissenberg, C. J., Klaver, M., de Graaff, S. J., Koornneef, J. M., Smeets, R. J., MacLeod, C.J., Davies, G. R. 2018. Isotopic variation in Semail Ophiolite lower crust reveals crustal-level melt aggregation. Geochem. Persp. Let. 8, 37-42. doi:10.7185/geochemlet.1827

826 Jousselin, D., Nicolas, A., Boudier, F., 1998. Detailed mapping of a mantle diapir below a
827 paleo-spreading center in the Oman ophiolite. J. Geophys. Res. Solid Earth 103, 18153-
828 18170. doi:10.1029/98JB01493
829 Kelemen, P.B., Shimizu, N., Dunn, T., 1993. Relative depletion of niobium in some arc
830 magmas and the continental crust: partitioning of K, Nb, La and Ce during melt/rock
831 reaction in the upper mantle. Earth Planet. Sci. Lett. 120, 111-134. doi:10.1016/0012-
832 821X(93)90234-Z
833 Koepke, J., Feig, S. T., Snow, J, 2005. Hydrous partial melting within the lower oceanic crust.
834 Terra Nova 17, 286-291. doi:10.1111/j.1365-3121.2005.00613.x
835 Koga, K.T., Kelemen, P.B., Shimizu, N., 2001. Petrogenesis of the crust-mantle transition
836 zone and the origin of lower crustal wehrlite in the Oman ophiolite. Geochemistry,
837 Geophys. Geosystems 2. doi:10.1029/2000GC000132
838 MacLeod, C.J., Rothery, D.A., 1992. Ridge axial segmentation in the Oman ophiolite:
839 Evidence from along-strike variations in the sheeted dyke complex. Ophiolites Their
840 Mod. Ocean. Analog. 60, 39-63. doi:10.1144/GSL.SP.1992.060.01.03
841 Nehlig, P., Juteau, T., 1988. Deep crustal seawater penetration and circulation at ocean ridges:
842 Evidence from the Oman ophiolite. Mar. Geol. 84, 209-228. doi:10.1016/0025-
843 3227(88)90102-8
844 Nicolas, A., Ceuleneer, G., Boudier, F., Misseri, M., 1988. Structural mapping in the Oman
845 ophiolites: Mantle diapirism along an oceanic ridge. Tectonophysics 151, 27-56.
846 doi:10.1016/0040-1951(88)90239-9
847 Pallister, J.S., 1981. Structure of the sheeted dike complex of the Samail Ophiolite near Ibra,
848 Oman. J. Geophys. Res. Solid Earth 86, 2661-2672. doi:10.1029/JB086iB04p02661
849 Python, M., Ceuleneer, G., 2003. Nature and distribution of dykes and related melt migration
850 structures in the mantle section of the Oman ophiolite. Geochemistry, Geophys.

851 Geosystems 4. doi:10.1029/2002GC000354
852 Python, M., Ceuleneer, G., Ishida, Y., Barrat, J.-A., Arai, S., 2007. Oman diopsidites: a new
853 lithology diagnostic of very high temperature hydrothermal circulation in mantle
854 peridotite below oceanic spreading centres. Earth Planet. Sci. Lett. 255, 289-305.
855 doi:10.1016/j.epsl.2006.12.030
856 Quick, J. E., 1981. The origin and significance of large, tabular dunite bodies in the Trinity
857 peridotite, northern California. Contrib. Mineral. Petrol. 78, 413-422.
858 doi:10.1007/BF00375203
859 Rabu, D., Béchennec, F., Beurrier, M., Hutin, M., 1986. Geological Map of Nakhl: Sheet NF
860 40-3E, Scale: 1:100,000. Explanatory Notes. Dir. Gen. Miner. Oman Minist. Pet. Miner.
861 Reuber, I., 1988. Complexity of the crustal sequence in the northern Oman ophiolite (Fizh
862 and southern Aswad blocks): The effect of early slicing? Tectonophysics 151, 137-165.
863 doi:10.1016/0040-1951(88)90244-2
864 Rioux, M., Bowring, S., Kelemen, P., Gordon, S., Miller, R., Dudás, F., 2013. Tectonic
865 development of the Samail ophiolite: High-precision U-Pb zircon geochronology and
866 Sm-Nd isotopic constraints on crustal growth and emplacement. J. Geophys. Res. Solid
867 Earth 118, 2085-2101. doi:10.1002/jgrb.50139
868 Rospabé, M., 2018. Etude pétrologique, géochimique et structurale de la zone de transition
869 dunitique dans l'ophiolite d'Oman : Identification des processus pétrogénétiques à
870 l'interface manteau/croûte. Université Paul Sabatier, Toulouse III.
871 Rospabé, M., Benoit, M., Ceuleneer, G., Hodel, F., & Kaczmarek, M. A., 2018a. Extreme
872 geochemical variability through the dunitic transition zone of the Oman ophiolite:
873 Implications for melt/fluid-rock reactions at Moho level beneath oceanic spreading
874 centers. Geochim. Cosmochim. Acta 234, 1-23. doi:10.1016/j.gca.2018.05.012
875 Rospabé, M., Benoit, M., Candaudap, F., 2018b. Determination of Trace Element Mass

876 Fractions in Ultramafic Rocks by HR-ICP-MS: A Combined Approach Using a Direct
877 Digestion/Dilution Method and Preconcentration by Coprecipitation. Geostand.
878 Geoanalytical Res. 42, 115–129. doi:10.1111/ggr.12181
879 Rospabé, M., Ceuleneer, G., Benoit, M., Abily, B., Pinet, P., 2017. Origin of the dunitic
880 mantle-crust transition zone in the Oman ophiolite: The interplay between percolating
881 magmas and high-temperature hydrous fluids. Geology 45, 471-474.
882 doi:10.1130/G38778.1
883 Sanfilippo, A., Tribuzio, R., Ottolini, L., Hamada, M., 2017. Water, lithium and trace element
884 compositions of olivine from Lanzo South replacive mantle dunites (Western Alps):
885 New constraints into melt migration processes at cold thermal regimes. Geochim.
886 Cosmochim. Acta 214, 51-72. doi:10.1016/j.gca.2017.07.034
887 Sanfilippo, A., Morishita, T., Kumagai, H., Nakamura, K., Okino, K., Hara, K., Tamura, A.,
888 Arai, S., 2015. Hybrid troctolites from mid-ocean ridges: Inherited mantle in the lower
889 crust. Lithos 232, 124-130. doi:10.1016/j.lithos.2015.06.025
890 Sanfilippo, A., Tribuzio, R., Tiepolo, M., 2014. Mantle-crust interactions in the oceanic
891 lithosphere: Constraints from minor and trace elements in olivine. Geochim.
892 Cosmochim. Acta 141, 423-439. doi:10.1016/j.gca.2014.06.012
893 Sinton, J., Bergmanis, E., Rubin, K., Batiza, R., Gregg, T.K.P., Gronvold, K., Macdonald,
894 K.C., White, S.M., 2002. Volcanic eruptions on mid-ocean ridges: New evidence from
895 the superfast spreading East Pacific Rise, 17 degrees-19 degrees S. J. Geophys. Res.
896 Solid Earth 107. doi:10.1029/2000JB000090
897 Sun S.-S. and McDonough W. F., 1989. Chemical and isotopic systematics of oceanic basalts:
898 implications for mantle composition and processes. Geol. Soc. Lond., Spec. Publ. 42,
899 313-345. doi:10.1144/GSL.SP.1989.042.01.19
900 Wyns, R., Béchennec, F., Chevrel, S., Le Métour, J., Roger, J., 1992. Geological Map of

Nazwa: Sheet NF 40-07, Scale: 1:250,000. Explanatory Notes. Dir. Gen. Miner. Oman Minist. Pet. Miner.

Yeo, I.A., Devey, C.W., LeBas, T.P., Augustin, N., Steinführer, A., 2016. Segment-scale volcanic episodicity: Evidence from the North Kolbeinsey Ridge, Atlantic. Earth Planet. Sci. Lett. 439, 81-87. doi:10.1016/j.epsl.2016.01.029

Zagrtdenov, N. R., Ceuleneer, G., Rospabé, M., Borisova, A. Y., Toplis, M. J., Benoit, M., & Abily, B., 2018. Anatomy of a chromitite dyke in the mantle/crust transition zone of the Oman ophiolite. Lithos, 312, 343-357. doi:10.1016/j.lithos.2018.05.012

Zhang, C., Koepke, J., France, L., Godard, M., 2017. Felsic Plutonic Rocks from IODP Hole 1256D, Eastern Pacific: Implications for the Nature of the Axial Melt Lens at Fast-Spreading Mid-Ocean Ridges. J. Petrol. 58, 1535-1565. doi:10.1093/petrology/egx064

Zihlmann, B., Müller, S., Coggon, R.M., Koepke, J., Garbe-Schönberg, D., Teagle, D.A., 2018. Hydrothermal fault zones in the lower oceanic crust: An example from Wadi Gideah, Samail ophiolite, Oman. Lithos 323, 103-124. doi:10.1016/j.lithos.2018.09.008

Figure 1

Click here to download Figure: Fig.1-GeologicalMap.pdf

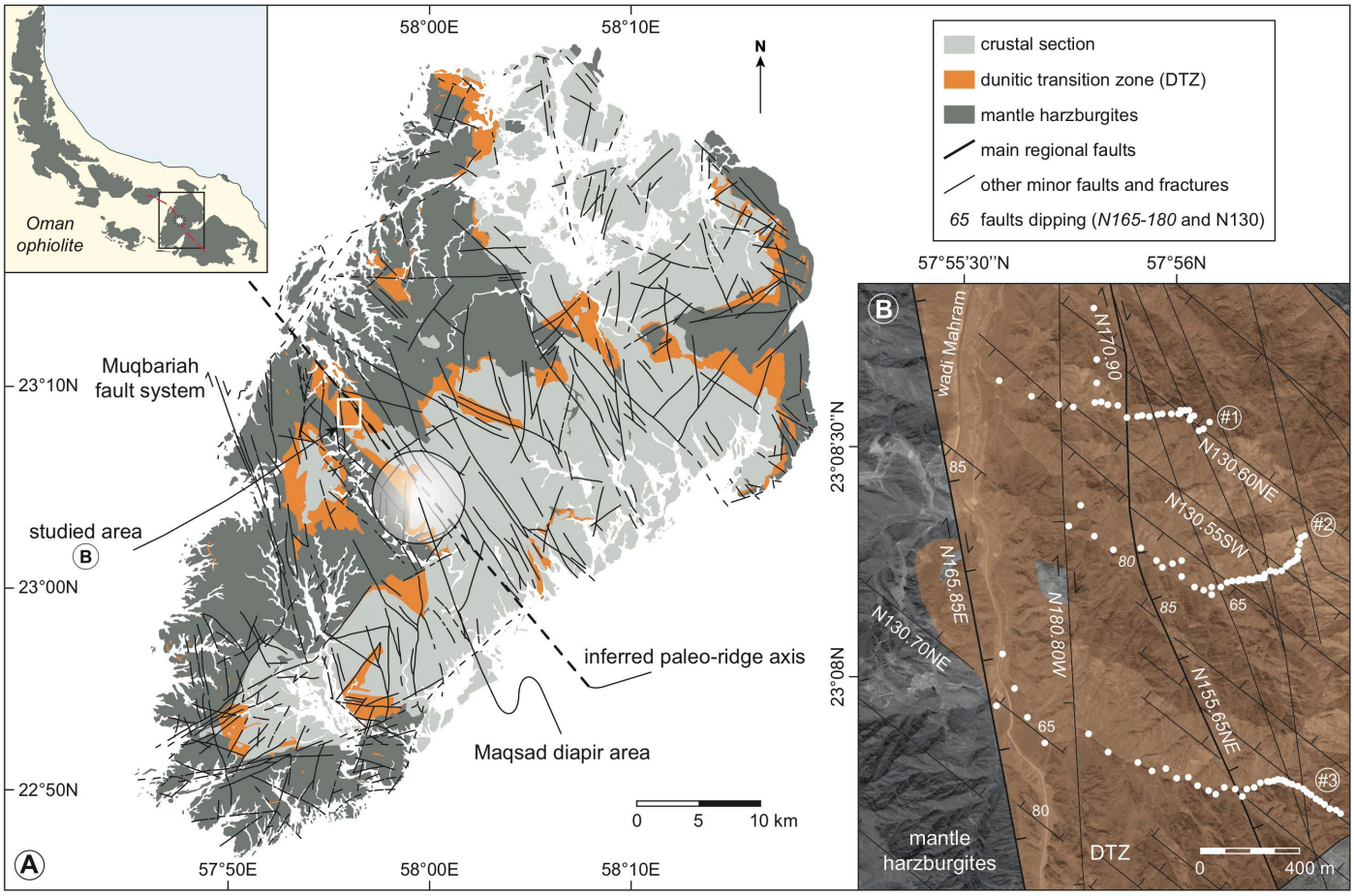

Figure 2

Click here to download Figure: Fig.2-FieldObservations.pdf

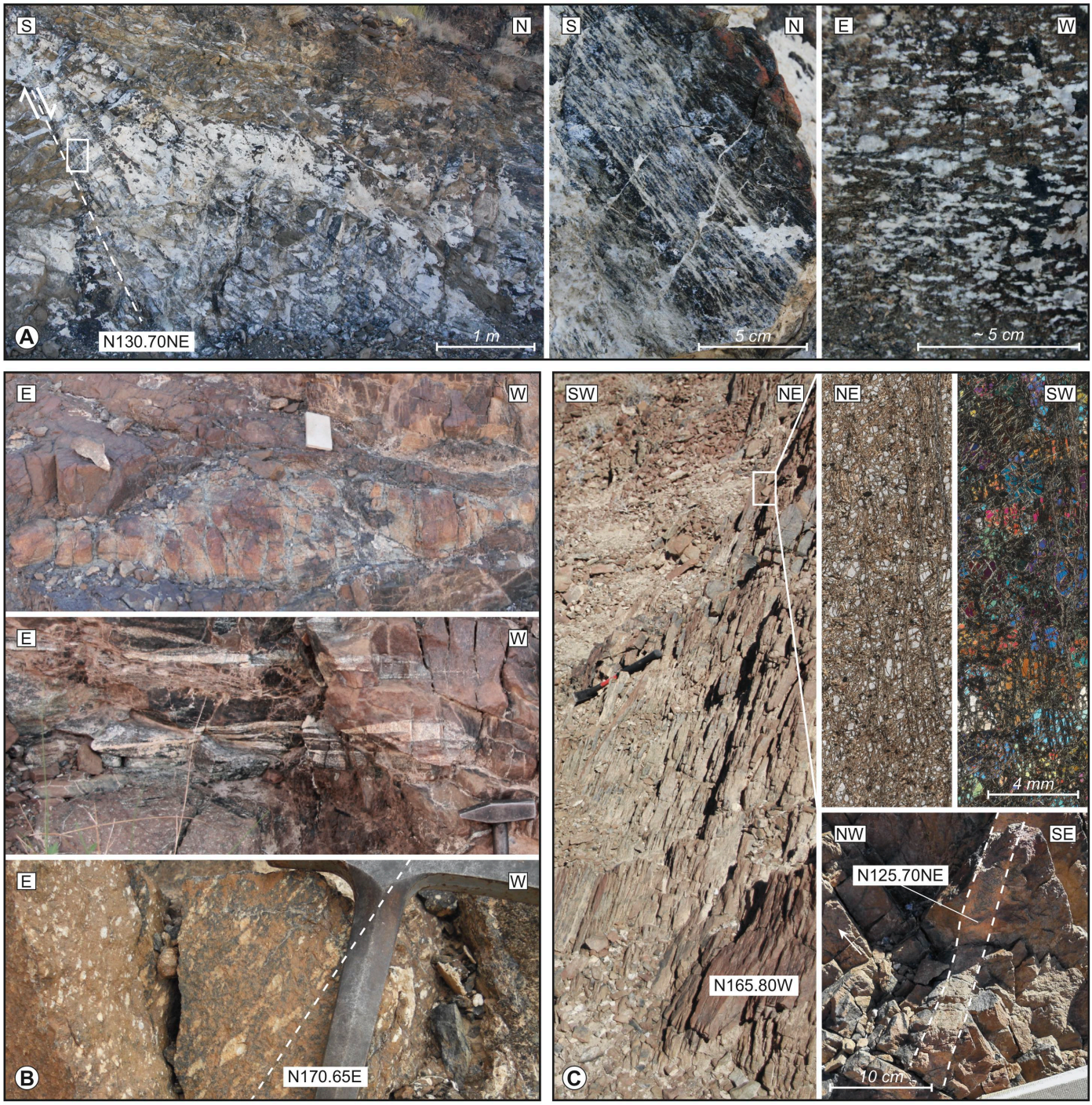

Figure 3

Click here to download Figure: Fig.3-Logs.pdf

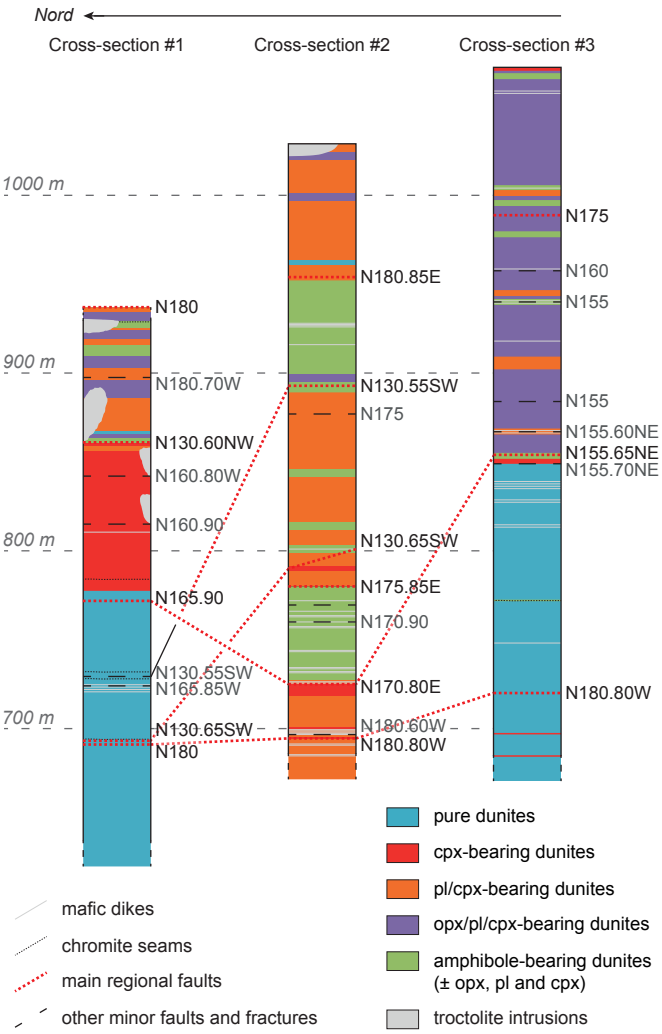

Figure 4

Click here to download Figure: Fig.4-ThinSections.pdf

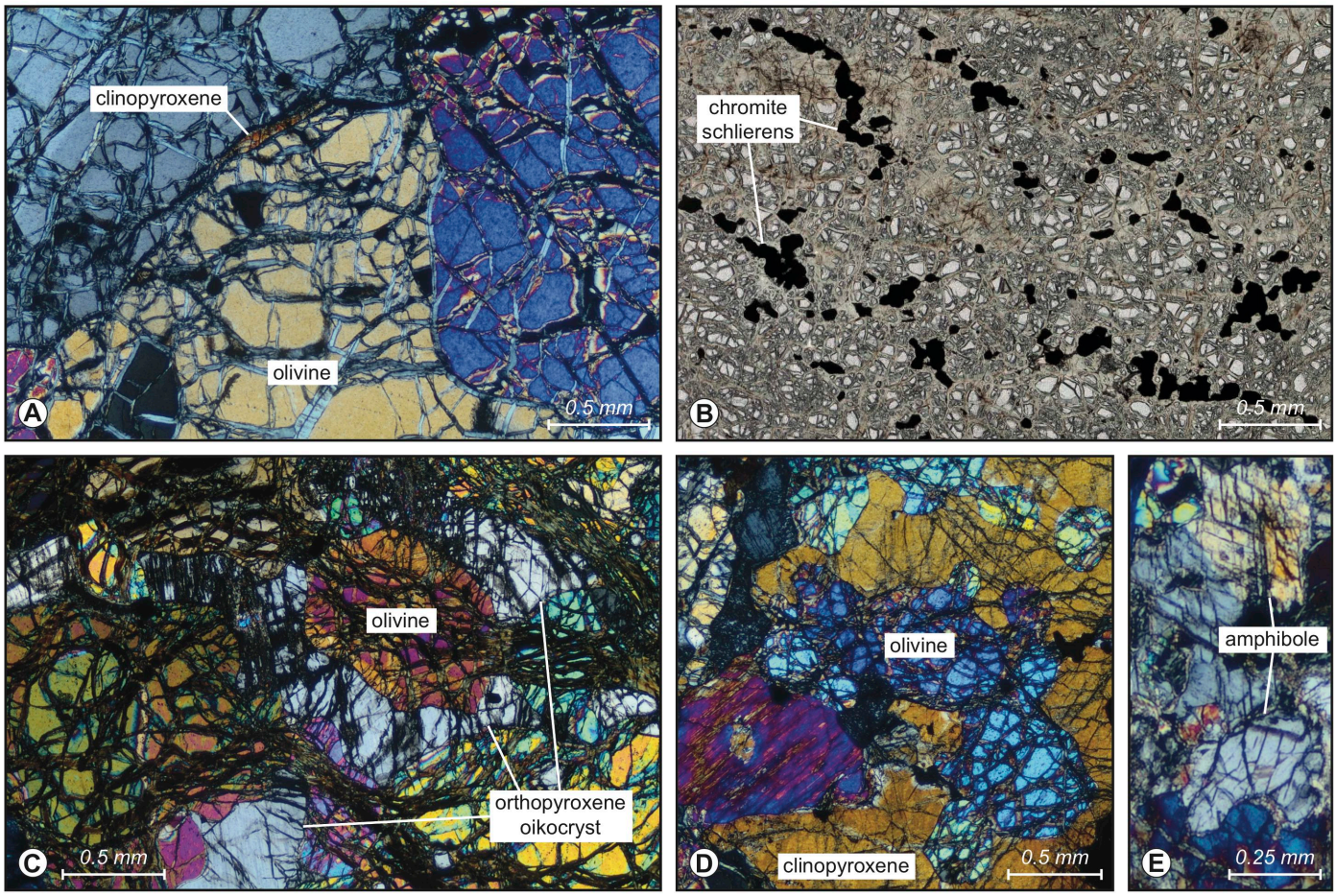

Figure 5

Click here to download Figure: Fig.5-GeochemistryDunites.pdf

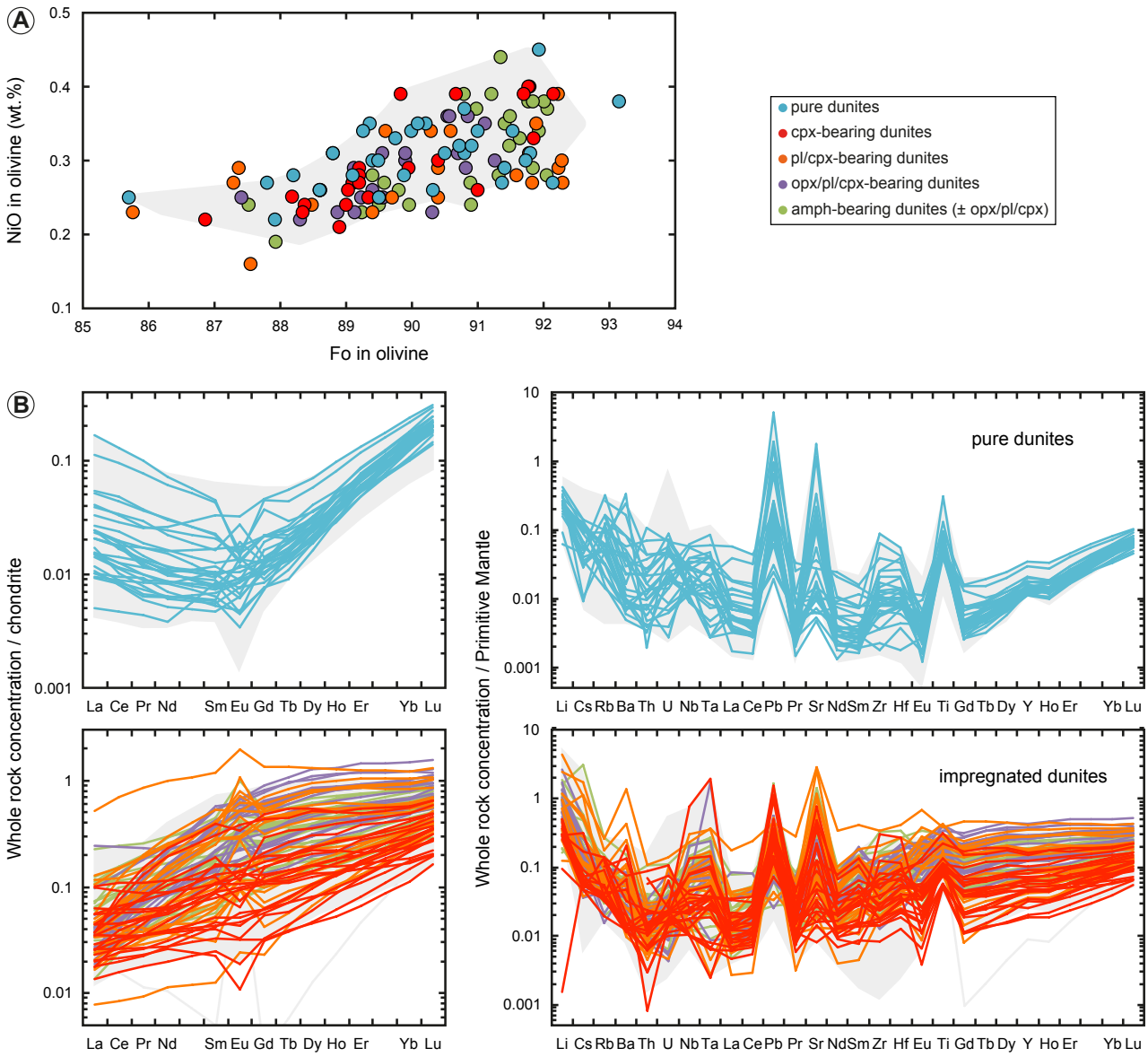

Figure 6

Click here to download Figure: Fig.6-GeochLogMnx.pdf

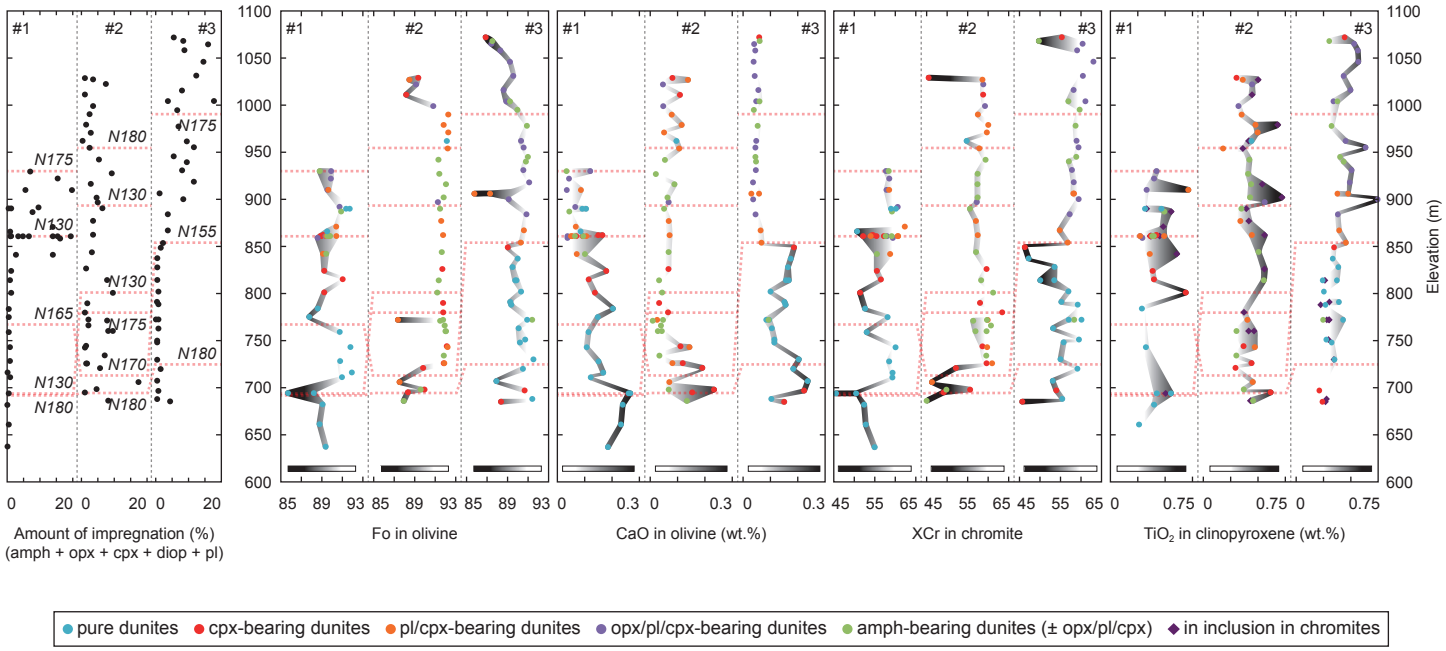

Figure 7

Click here to download Figure: Fig.7-GeochLogWR.pdf

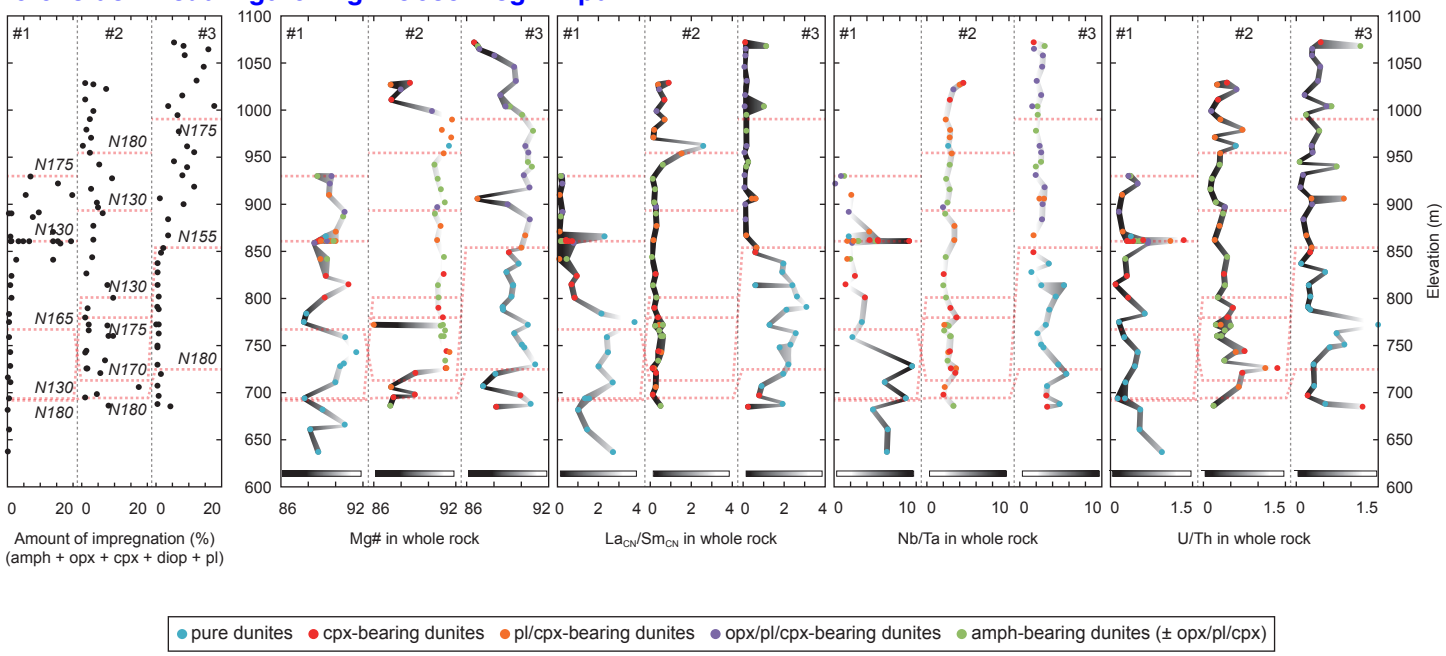

Figure 8

Click here to download Figure: Fig.8-CpxProfiles.pdf

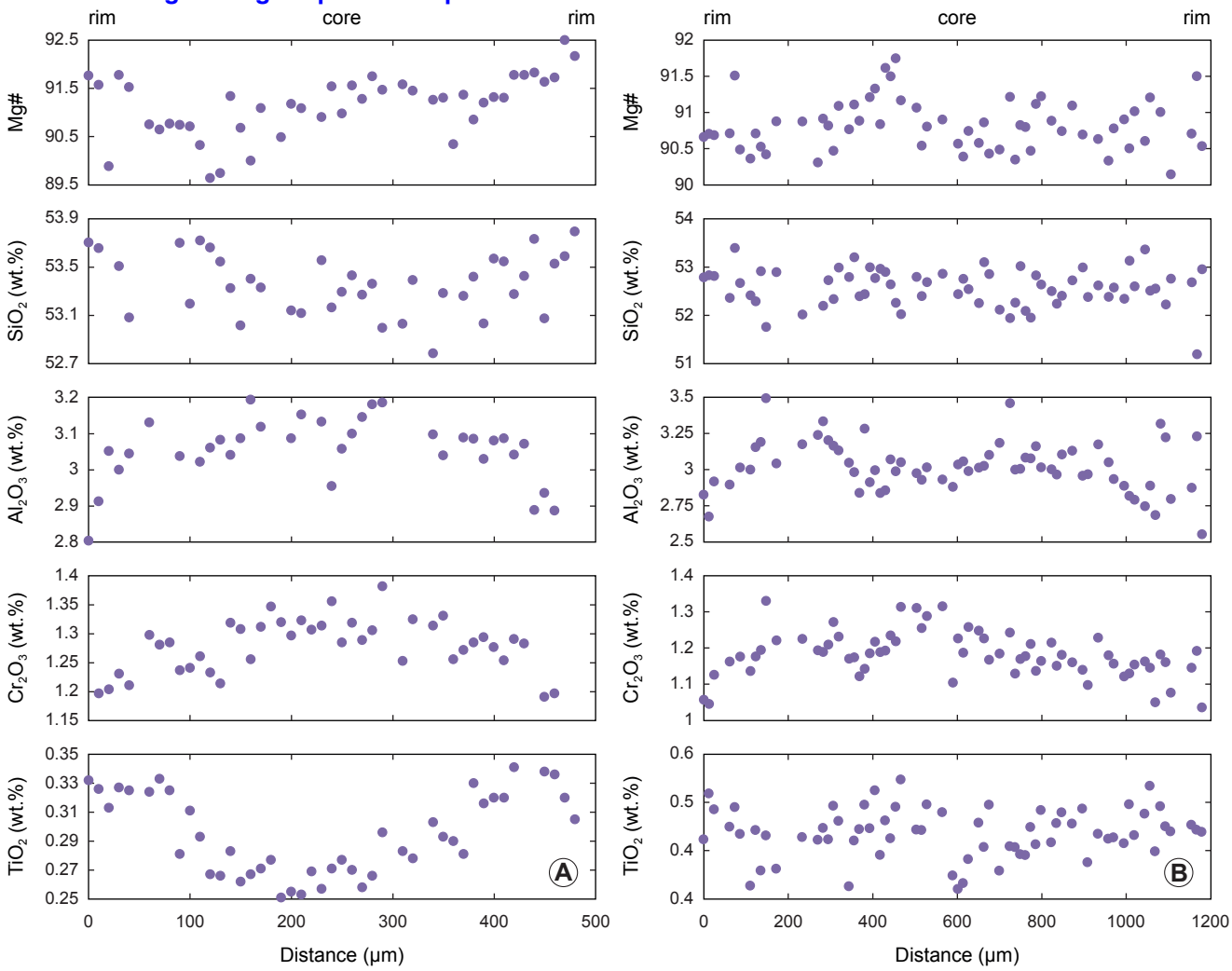

Figure 9

Click here to download Figure: Fig.9FinalSketch.pdf